J Solid State Electrochem (2007) 11:1549–1557
DOI 10.1007/s10008-007-0354-9

ORIGINAL PAPER

An analysis of X-ray absorption spectra in the XANES region of platinum-based electrocatalysts for low-temperature fuel cells

Ruy Sousa Jr. · Flávio Colmati · Eduardo Gonçalves Ciapina · Ernesto Rafael Gonzalez

Received: 30 January 2007 / Revised: 9 April 2007 / Accepted: 3 May 2007 / Published online: 1 June 2007

Abstract The knowledge of the electronic state of Pt-based electrocatalysts used in low temperature fuel cells is very important for the understanding of the activity of the material. Near-edge X-ray absorption spectroscopy (XANES), a particular region of the X-ray absorption spectra (XAS), can provide the desired information, but the analysis is not straightforward, particularly for the non-specialist. Mansour et al. (J. Phys. Chem., 88:2330, 1984) and Shukla et al. (J. Electroanal. Chem., 563:181, 2004) presented methods to obtain information on electronic states from XANES spectra. In this work, procedures to implement the two methods are presented in detail and applied to XANES results for Pt_2Sn_1/C and Pt/C electrocatalysts prepared in this laboratory. The scope and limitations of the two methods are also discussed. The results show that the presence of Sn in the Pt_2Sn_1/C material promotes a partial filling of the Pt 5d band, in comparison to Pt/C, which contributes to explain the better activity of the bimetallic material.

Keywords Platinum catalysts · Electrocatalysis · X-ray absorption · XANES

Introduction

Modern society is facing the problems of increasing demands for energy, and one of the most serious is an increasing degradation of the environment through the generation of pollutants coming from inefficient energy conversion methods. In this scenario, fuel cells appear as an attractive alternative for the conversion of energy with little or no effect on the environment.

Among low-temperature fuel cells (<200 °C), proton exchange membrane fuel cells (PEMFC) are able to produce high-power densities, which make them suitable for stationary, portable, and transportation applications. Additionally, PEMFC can operate with different fuels, like hydrogen, low-molecular-weight alcohols, and other organic compounds. The fuel cell works by oxidizing the fuel at the anode and reducing oxygen at the cathode, and except for the oxidation of hydrogen, these processes are characterized by a slow kinetics that requires the use of suitable catalysts. In the anode, the main function of the catalyst is to promote the adsorption of reagents and the oxidation of poisoning intermediates like CO. In the cathode, the catalyst must promote the adsorption and the reduction of oxygen, an intrinsically slow reaction, which proceeds more slowly when oxides/hydroxides are formed on the surface of the catalyst due to the high potential. Both adsorption and electron transfer processes on the catalyst surface depend strongly on electronic effects, that is, the degree of vacancy of the atomic orbitals that participate in those processes.

X-ray absorption spectroscopy (XAS) has the ability of probing the electronic and structural characteristics of electrocatalysts under in situ electrochemical conditions. In the near-edge energy region (X-ray absorption near-edge spectroscopy, XANES), it probes the ground-state unoccupied density of states of the crystal [1]. Synchrotron techniques necessary to obtain XAS spectra are becoming more available as new facilities are installed around the world. Thus, they are available not only to the XAS specialist but also to scientists working in catalysis

This paper is dedicated to Prof. Francisco Nart, in memoriam.

R. Sousa Jr. · F. Colmati · E. Ciapina · E. R. Gonzalez (✉)
Instituto de Química de São Carlos (IQSC),
Universidade de São Paulo (USP),
Av. Trabalhador Sãocarlense, 400, C.P. 780,
13560-970 São Carlos, SP, Brazil
e-mail: ernesto@iqsc.usp.br

that want to derive important information on the materials being studied by the use of XAS techniques. Electrocatalysts for low-temperature fuel cells and, in particular for PEMFC, are usually based on platinum or platinum alloys with transition elements. For the non-XAS specialist, the interpretation of XANES spectra to derive the desired information may be an arid process, so the purpose of this work is to analyze the available techniques for the interpretation of XANES spectra, having in mind the information relevant for catalysis, and present them in a clear way.

The large peak called white line, visible in many L- and K-edge spectra, has been understood as due to a high density of final states. The L_1 edge initiates from the 2s state, while the $L_{2,3}$ edges initiate from the 2p state, probing the density of final states with different symmetries. The L_1 edge is associated with the p-symmetric portion of the density of final states, while the $L_{2,3}$ edges are associated with the s- and d-symmetric portions. The s-symmetric portion of the density of states is usually small and spread in energy (white lines are not expected from this symmetry). However, the d-symmetric portion of the density of states can be large and narrow, being a candidate to produce well-defined white lines [2].

For platinum, the L_1 edge does not produce a white line, as it is usual for a transition metal, and also the L_2 edge does not produce a significant white line. The L_3 edge, on the other hand, produces a prominent white line [3]. As hybridization of d states becomes weaker, the peak at the L_3 threshold is enhanced and that at the L_1 is depressed. The large intensity of the peak at the L_3 edge of transition metals is due to the atomic-like character of the d resonance in transition metals [1]. The ability of XAS to probe the absorption edges of Pt-based electrocatalysts under in situ electrochemical conditions using the near-edge part of the spectra can provide a direct measure of their d-band vacancies that are related to the activity of the catalyst [4]. In this context, the availability of suitable practical techniques for the analysis of experimental data becomes very important.

Two different methods can be considered for the analysis of white lines associated with platinum-based catalysts: One was proposed by Mansour et al. [5] and was extensively used by other authors [6–8], and the other one was considered by Shukla et al. [9]. In this work, we apply the two techniques to the analysis of some XANES experimental data from our laboratory, discuss the information gathered by the two methodologies, and perform some critical analysis of the results.

Background

Considering first the work by Mansour et al. [5], we recall that the absorption of an X-ray photon results in a photoelectron being emitted with kinetic energy, E. In this process, the total absorption coefficient, μ, can be expressed as

$$\mu x = \ln(I_0/I), \tag{1}$$

where x is the absorber thickness, I_0 is the intensity of the incident beam, and I is the intensity of the transmitted beam.

The total X-ray absorption coefficient, μ, may be written as

$$\mu = \mu_{Li} + \mu', \tag{2}$$

where μ_{Li} is the absorption coefficient for the electrons that undergo transitions corresponding to the L_2 or L_3 edges and μ' is the absorption coefficient for all other electrons in the system. It is then assumed that μ_{Li} may be written as

$$\mu_{Li} = \mu_{di} + \mu_{si}, \tag{3}$$

where μ_{di} is the contribution due to the unoccupied d states and μ_{si} is the contribution due to the unoccupied s states.

To apply the procedure described in [5], the form of $\mu_{\mathrm{si}}(E)$ is approximated by an appropriate L-edge spectrum (e.g., a Pt foil L_2-edge spectrum) of another element that does not present a significant white line. It must be pointed out that there is some uncertainty in scaling and positioning the energy of this edge, but this can be done by comparisons that take into account the extended X-ray absorption fine structure (EXAFS) region. Finally, the approximated form of $\mu_{\mathrm{si}}(E)$ is subtracted from $\mu_{\mathrm{Li}}(E)$ to obtain $\mu_{\mathrm{di}}(E)$. In this sense, the areas A_2 and A_3 (see Fig. 1a and b) that will be used to extract the information about the unoccupied states are defined as

$$A_2 = \int \left(\mu_{L_2} - \mu_{s_2}\right) dE \tag{4a}$$

$$A_3 = \int \left(\mu_{L_3} - \mu_{s_3}\right) dE \tag{4b}$$

In Fig. 1a and b, μ_{si} corresponds to manually added arc tangent (quasi)continuous functions (only for illustration purposes). $A2$ and $A3$ are associated with the probabilities of transition [10, 11], given by an interaction operator f, from initial states, $<a|$, to determined final states, $|b>$, which are proportional to

$$|\langle a|f|b\rangle|^2 \tag{5}$$

but,

$$|\langle a|f|b\rangle|^2 \alpha (2j'+1) \sum_{lj} A_{lj}^{n'l'j'} \tag{6a}$$

with

$$A_{lj}^{n'l'j'} = \frac{1}{4}\left(\frac{1}{j'+1}\delta_{l,l'+1}\delta_{j,j'+1} + \frac{1}{j'(j'+1)(2j'+1)}\delta_{l,l'+1}\delta_{j,j'} + \frac{1}{j}\delta_{l,l'-1}\delta_{j,j'-1}\right)\left[R_{lj}^{n'l'j'}\right]^2 \quad (6b)$$

where $n'l'j'$ and lj are the quantum numbers, the coefficients $A_{lj}^{n'l'j'}$ are slowly varying functions of the energy, the terms δ are associated with the dipole selection rule ($\Delta l = \pm 1, \Delta j = 0, \pm 1$) and $R_{lj}^{n'l'j'}$ is the radial dipole moment integral. The values [3] of $(2j'+1)A_{lj}^{n'l'j'}/(R_{lj}^{n'l'j'})^2$ associated with the L_2 edge are 0 (j=5/2) and 5/15 (j=3/2), and those associated with the L_3 edge are 6/15 (j=5/2) and 1/15 (j=3/2). Therefore,

$$A_2 = C'\left(R_d^{2p1/2}\right)^2\left(\frac{5}{15}h_{3/2}\right) \quad (7a)$$

$$A_3 = C'\left(R_d^{2p3/2}\right)^2\frac{\left(6h_{5/2}+h_{3/2}\right)}{15}, \quad (7b)$$

where C′ is a numerical constant, R_d is the radial part in the dipole transition matrix element connecting the core states $n'l'j'$ with the d states, and the $h_j's$ are the number of unoccupied d states characterized by quantum number j.

Because the degeneracy of the $2p_{3/2}$ states is twice the value for the $2p_{1/2}$ states, the areas should differ by a factor of 2 before normalization. However, due to differences in the radial part of the dipole transition matrix, the L_2 absorption edge should be multiplied by 2.22 (in agreement with results already discussed [3]). Considering this difference between the areas for the L_2 and the L_3 absorption edges, the expressions for the areas are

$$A_2 = C\left(\frac{1}{3}h_{3/2}\right) \quad (8a)$$

$$A_3 = C\frac{\left(6h_{5/2}+h_{3/2}\right)}{15}\left(\frac{2.22}{2}\right) \quad (8b)$$

$$C = C'\left(R_d^{2p1/2}\right)^2$$

By solving for h_j,

$$h_{3/2} = \frac{3A_2}{C} \quad (9a)$$

$$h_{5/2} = \frac{(2.25A_3 - 0.5A_2)}{C} \quad (9b)$$

$$h_T = h_{3/2} + h_{5/2} = \frac{2.25(A_3 + 1.11A_2)}{C} \quad (9c)$$

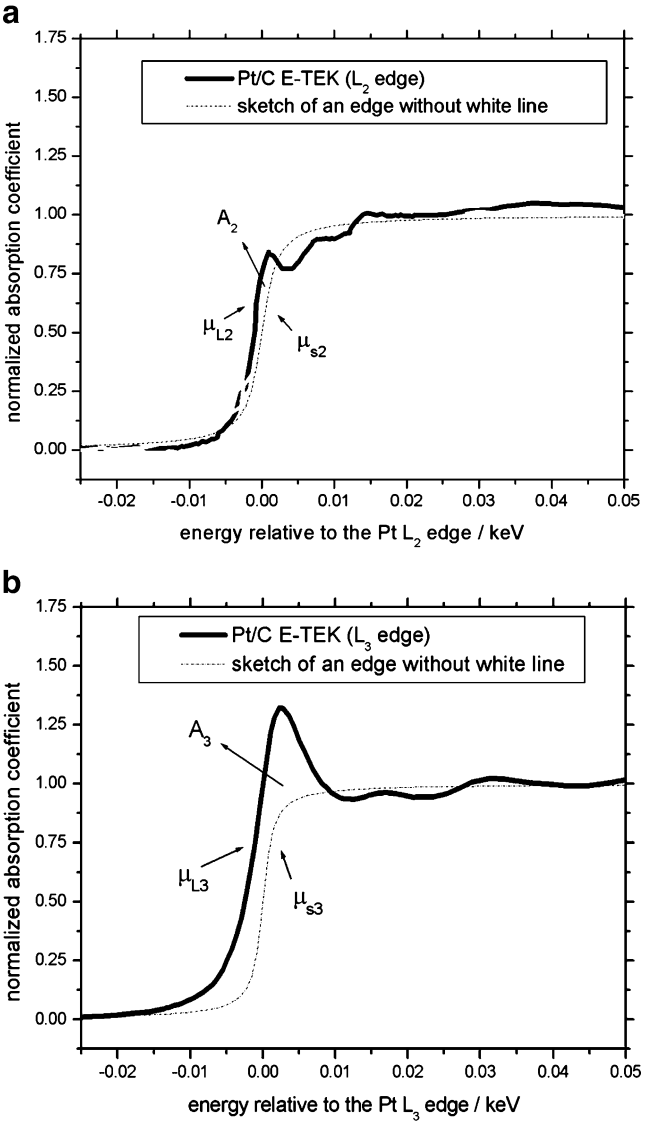

Fig. 1 **a** L_2 absorption edge for Pt/C E-TEK in comparison with $\mu_{S2}(E)$. **b** L_3 absorption edge for Pt/C E-TEK in comparison with $\mu_{S3}(E)$

The difficulty in determining the areas A_2 and A_3 arises because $\mu_{si}(E)$ is not measurable experimentally. Besides, it is also very difficult to determine the value of the constant C in the above equations.

The method proposed by Mansour et al. [5] is based on the evaluation of the fractional change in the number of d-band vacancies relative to a reference material, instead of attempting to evaluate the absolute total number of unoccupied states. For this purpose, the ratio fd is defined as

$$fd = \frac{(h_{Ts} - h_{Tr})}{h_{Tr}} = \frac{(\Delta A_3 + 1.11\Delta A_2)}{A_{3r} + 1.11A_{2r}} \quad (10a)$$

with

$$\Delta A_3 = A'_{3s} - A'_{3r} \text{ and } \Delta A_2 = A'_{2s} - A'_{2r}, \quad (10b)$$

where the subscript s refers to the sample and r refers to the reference material [primes in Eq. 10b denote total areas, i.e., under $\mu_{di}(E)+\mu_{si}(E)$]. The quantity $(A_{3r}+1.11A_{2r})$ is a constant for a given element. It can be determined by following the procedure presented in [2] (see also [3, 5, 12]).

From 10a,

$$h_{Ts} = (1 + fd)h_{Tr} \tag{11}$$

The h_{Ts} can be calculated from Eq. 11 in the following way: By integrating the total areas under $\mu_{L2}(E)$ and $\mu_{L3}(E)$, for the sample and the reference materials, the edge areas of interest, $A'_{3s}, A'_{3r}, A'_{2s}$, *and* A'_{2r}, to apply Mansour's method can be obtained. They are determined by numerical integration using Simpson's rule $\left(\int f(x)dx = h(1/3f(x1)+ 1/3f(x2)+ 1/3f(x3))) 1/3f(x3))\right)$. In this way, $(\Delta A_3+1.11\Delta A_2)$ is calculated. The areas must be normalized by multiplying by $\sigma\rho$, where σ is the X-ray absorption cross-section at the edge jump and ρ is the density of the absorbing material (see "Results and discussion" for the values of σ and ρ used in this work). As mentioned above, the quantity $(A_{3r}+1.11A_{2r})$ is a constant for a given element [5] and allows to calculate the ratio $fd = \frac{(\Delta A_3+1.11\Delta A_2)}{A_{3r}+1.11A_{2r}}$. Finally, by considering that h_{Tr} can be evaluated from a band structure calculation [2], h_{Ts} is obtained by applying Eq. 11.

However, to correctly apply the method of Mansour et al. [5] by following the above procedure, some steps must be performed beforehand with the experimental results [13, 14]:

1. The energy scale is shifted so that the position of the edge (inflection point on the absorption edge step) corresponds to zero.
2. A pre-edge smooth background function must be subtracted from the entire range of the data to remove the contribution of all other electrons to the absorption spectrum.
3. To allow that the EXAFS regions of different edges overlap one another (in terms of the amplitude of the oscillations), a fitted post-edge function can be subtracted from the EXAFS region data to remove the very low frequency components. Next, the data must be normalized. The normalization value is chosen as the absorbance at the inflection point of one of the EXAFS oscillations. A spectrum is normalized by dividing each data point by the normalization value.
4. Finally, the L_2 absorption edge spectrum can be further shifted by adjusting the energy scale (as in step 1) so that the EXAFS oscillations in both the L_2 and L_3 edges align with each other. The same procedure can also be used to align (in the energy) the L_2 and L_3 edges of the sample with the L_2 and L_3 edges of the reference material.

The other practical technique for the analysis of white lines of platinum-based catalysts is the method considered by Shukla et al. [9]. The removal of a pre-edge background is performed by fitting a polynomial function to the data in the range from −300 to −50 eV from the inflexion point and then extending it over the energy range of interest, followed by the subtraction from the considered data set. The proper way of performing the normalization was discussed by Wong et al. [15]. Again, the normalization value is referred to the absorbance at the inflection point of one of the EXAFS oscillations. The absorption spectra could then be fitted to a Lorentzian curve after subtracting an arc tangent function that, according to Richtmeyer et al. [16], corresponds to $\mu_{si}(E)$ if Fermi–Sommerfeld levels are considered equally distributed. The arc tangent function is given by:

$$\mu_{si}(E) = C''\left\{\frac{1}{2} - \frac{1}{\pi}\arctan\left(\frac{\upsilon_{E_0A} - \upsilon}{\Gamma_E/2}\right)\right\} \tag{12}$$

where C'', υ_{E_0A} and Γ_E are constants.

The integrated intensity given by the Lorentzian supplies information about the d-band vacancies for platinum-based catalysts

$$y = y0 + 2\frac{A}{\pi}\frac{w}{\left[4(x - xc)^2 + w^2\right]}, \tag{13}$$

where $y0$ is an "offset" term, A is the total area under the curve, xc is the peak center, and w is the peak width at half height.

Materials and methods

The platinum-based materials considered in this work were supported catalysts used in low-temperature fuel cells: 20 wt% platinum on carbon (Pt/C) from E-TEK and 20 wt% platinum–tin metal on carbon (Pt_2Sn_1/C) prepared in this laboratory. The raw materials consist of platinum or platinum alloy nanosize particles (2–6 nm) supported on high-surface-area carbon. The Pt_2Sn_1/C electrocatalyst was prepared in this laboratory by the so-called formic acid method (FAM) [17]. An appropriate mass of carbon powder (Vulcan XC-72, Cabot, 240 m^2 g^{-1}) was suspended in a 2-mol l^{-1} formic acid solution and the suspension heated up to 80°C. Chloroplatinic acid (H_2PtCl_6. $6H_2O$, Johnson Matthey) and tin chloride ($SnCl_2$. $2H_2O$, Merck) solutions were added slowly to the carbon suspension. The suspension was left to cool at room temperature, and the solid filtered and dried in an oven at 80°C for 1 h. The atomic ratios of the Pt_2Sn_1/C catalysts were determined by energy dispersive X-ray analysis (EDX) coupled to a scanning electron microscope, LEO Mod. 440, with a silicon detector with Be

window and applying 20 keV. X-ray diffractograms (XRD) were obtained at the XRD beam line at the Brazilian Synchrotron Light Source Laboratory, LNLS, in Brazil. The diffractograms were obtained in the reflection mode URD-6, operating with Cu k_α radiation (λ=0.15406 nm). The scans were performed at 3° min^{-1} for 2θ values between 30 and 100°. To estimate the crystallite size of Pt/C E-TEK and Pt_2Sn_1/C from XRD, the Scherrer equation was used [18]. For this purpose, the (220) peak of the Pt fcc (face–centred–cubic) structure around 2θ=70° was selected (because the broad carbon peak does not interfere in this region). The lattice parameters were obtained by refining the unit-cell dimensions by the least squares method [19]. Further details on the PtSn materials, like alloy formation, can be found elsewhere [20]. Working electrodes containing 6 mg cm^{-2} of platinum were made by agglutinating the material into pellets with a 40 wt% dispersion of PTFE. These electrodes were conditioned in a homemade spectroelectrochemical cell [21].

The XAS measurements were performed at the XAS beam line at the Brazilian Synchrotron Light Laboratory, LNLS, in Brazil. The data acquisition system for the XAS experiments comprised three ionization detectors (incidence, I_0; transmitted, I_t; and reference, I_r). The reference channel was employed for internal calibration of the edge positions by using a Pt foil. The counter electrode was prepared in the same way as the working electrode, but using a commercial carbon supported platinum (Pt/C E-TEK) catalyst. The center of this electrode was cut to allow the free passage of the X-ray beam. Before the experiments, the electrodes were soaked in the electrolyte for 48 h. For activation, the electrode was cycled between 100 and 700 mV vs reversible hydrogen electrode (RHE) before the X-ray absorption measurements. All measurements were performed at 1,100 mV (with respect to a RHE) in a 0.5-mol l^{-1} H_2SO_4 electrolyte. A PAR 273-A potentiostat was used for the potential control. Above 800 mV vs RHE, oxygenated species are adsorbed on the Pt/C electrocatalyst, and this increases the white line [22, 23]. The white line is sensitive to the electrode potential, but there is a limit because, above 1,100 mV, the alloy can be degraded by oxidative processes that affect the metal and the carbon substrate. In this work, the results are shown at 1,100 mV because the differences among the spectra of the materials are larger at this potential. No experiments were done at more positive potentials. An average of two spectra was used in the analysis to reduce noise, although the reproducibility was found to be good.

The computer program employed for the analysis of XAS data according to the method of Mansour et al. [5] was the WINXAS package [24]. Regarding the method of Shukla et al. [9], after the normalization and background removal, the absorption spectra were fitted by arc tangent and Lorentzian functions. To fit the functions, the Levenberg–Marquardt nonlinear regression method was used [25].

Results and discussion

Pt/C catalyst

Initially, the integration method of Mansour et al. [5] was applied for the quantitative analysis of white lines obtained with Pt/C E-TEK at 1,100 mV. The reference material was a Pt foil. Figure 2 shows the comparison of the L_2 edges for the sample and the reference material after applying the procedures described above to the experimental data.

By integrating the total areas under $\mu_{L2}(E)$ for the sample and the reference materials within an energy interval around the edge (from −0.03 to 0.01 keV), i.e., excluding the EXAFS region, the results were:

$$Sample : A'_{2s} = 0.01229 keV$$

$$Reference : A'_{2r} = 0.01063 keV$$

$$\Delta A_2 = 0.00166\, keV = 1.66\, eV$$

Figure 3, in turn, shows the comparison of the L_3 edges for the sample and the reference material.

By integrating the total areas under $\mu_{L3}(E)$ (within an energy interval around the edge from −0.04 to 0.01 keV, i.e., excluding the EXAFS region), for the sample and the reference materials, the results were:

$$Sample : A'_{3s} = 0.0149\, keV$$

$$Reference : A'_{3r} = 0.01451\, keV$$

$$\Delta A_3 = 0.00039\, keV = 0.39\, eV$$

The areas were normalized by multiplying by $\sigma\rho$, where σ is the X-ray absorption cross-section at the edge jump and ρ is the density of the absorbing material (21.5 g cm^{-3}). Values of 117.1 and 54.2 cm^2 g^{-1} were used for the absorption cross-sections at the L_3 and L_2 edges, respectively [26]. The resulting normalized values were $\Delta A2$= 1,934.398 eV cm^{-1} and $\Delta A3$=981.8835 eV cm^{-1}. Besides, $(A_{3r} + 1.11\, A_{2r}) = 1.92 \times 10^4\, eV\, cm^{-1}$ [5]. By applying Eq. 10, fd=0.1630, and by applying Eq. 11 and considering that hTr=0.3 [2], the result was $h_T(Pt/C\ E-TEK) =$ 0.3489.

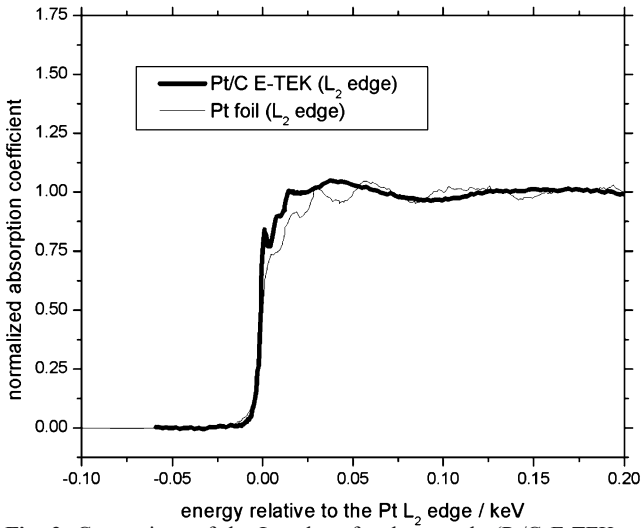

Fig. 2 Comparison of the L_2 edges for the sample (Pt/C E-TEK at 1,100 mV) and the reference material (Pt foil)

To apply the method of Shukla et al. [9], the absorption spectrum for the Pt foil was fitted with a Lorentzian curve after subtracting an arc tangent function (actually, the software considers a finite number of points to represent all fitted functions) in the form of Eq. 12, with constants $C'' = 1.01, \upsilon_{E_0A} = 0$ *and* $\Gamma_E = 0.00262$ keV. Figure 4a shows the arc tangent function. It is relevant to point out that the arc tangent function parameters are not arbitrary. The value of C″ must be close to 1, as it represents an asymptotic ordinate for high energies. Γ_E, in turn, is associated with the separation, in energy, of the two points where the normalized spectrum reaches one fourth and three fourths, respectively, of C″. Finally, υ_{E_0A} must be close to zero because it is associated with the inflection point on the absorption edge step. Some errors arise, of course, because of the fitting procedures, but the results obtained are very satisfactory ($C'' \approx 1, \upsilon_{E_0A} = 0$, and the error found for Γ_E was±0.0007 keV). Figure 4b shows the fitted Lorentzian, and the result obtained for the integrated intensity of the Lorentzian was 3.97 eV. For Pt/C E-TEK at 1,100 mV, after subtracting an arc tangent curve in the form of Eq. 12 with constants $C'' = 0.96, \upsilon_{E_0A} = 0$ and Γ_E= 0.00167 keV (again, $C'' \approx 1, \upsilon_{E_0A} = 0$ and the error for Γ_E was±0.0007 keV), a Lorentzian curve was fitted. The integrated intensity of the Lorentzian was 7.94 eV (see Fig. 5a and b).

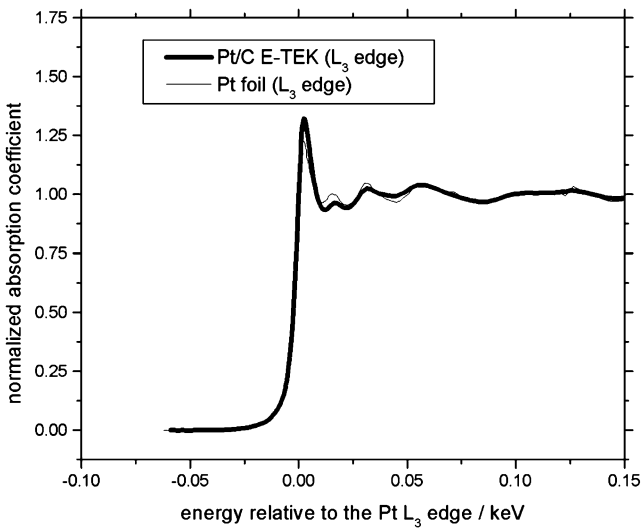

Fig. 3 Comparison of the L_3 edges for the sample (Pt/C E-TEK at 1,100 mV) and the reference material (Pt foil)

Pt_2Sn_1/C catalyst

The integration method of Mansour et al. [5] was also applied to the quantitative analysis of white lines associated to the Pt_2Sn_1/C catalyst, prepared in this laboratory, at 1,100 mV vs RHE. The reference material was also a Pt foil. Figure 6 shows the comparison of the L_2 edges for the sample and the reference material.

By integrating the total areas under $\mu_{L2}(E)$ for the sample and the reference materials, the results were:

$$Sample : A'_{2s} = 0.01124\, keV$$

$$Reference : A'_{2r} = 0.01063\, keV$$

$$\Delta A_2 = 0.00061\, keV = 0.61\, eV$$

Figure 7, in turn, shows the comparison of the L_3 edges for the sample and the reference material.

By integrating the total areas under $\mu_{L3}(E)$ for the sample and the reference materials, the results were:

$$Sample : A'_{3s} = 0.01462\, keV$$

$$Reference : A'_{3r} = 0.01451 \text{keV}$$

$$\Delta A_3 = 0.00011\, keV = 0.11\, eV$$

In terms of the normalized values, $\Delta A2$=710.833 eV cm^{-1} and $\Delta A3$=276.9415 eV cm^{-1}. Again, $(A_{3r} + 1.11A_{2r}) = 1.92 \times 104\, eV\ cm^{-1}$ [5]. By applying Eq. 10, fd=0.0555. And by applying Eq. 11, and considering that hTr=0.3 [2], the result was hT(Pt_2Sn_1/C)=0.3167.

Applying the method of Shukla et al. [9], the absorption spectrum for Pt_2Sn_1/C at 1,100 mV was fitted to a Lorentzian curve after subtracting an arc tangent in the form of Eq. 12, with constants $C'' = 1.01, \upsilon_{E_0A} = 0$ and 0.00234 keV (again, $C'' \approx 1, \upsilon_{E_0A} = 0$ and the error

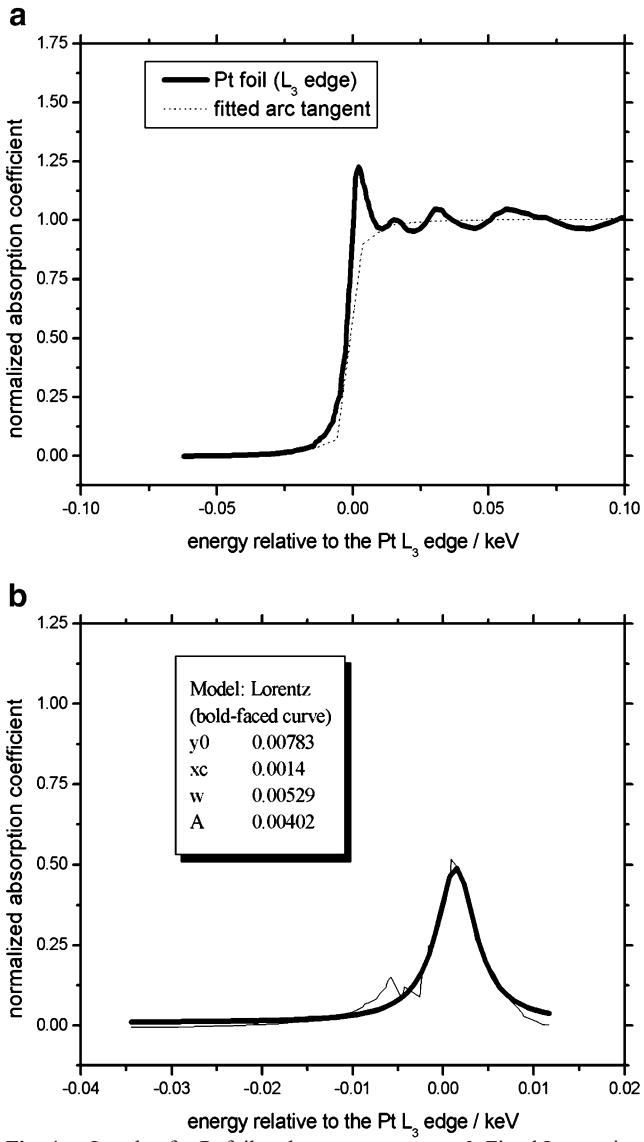

Fig. 4 **a** L_3 edge for Pt foil and arc tangent curve. **b** Fitted Lorentzian for the Pt foil

for $\Gamma_E = \pm 0.0007\,keV$). Figure 8a shows the arc tangent function. Figure 8b shows the fitted Lorentzian, and the result obtained for the integrated intensity of the Lorentzian was 6.98 eV.

Summing up, the analysis carried out with the method of Mansour et al. [5] gave the following results for the number of unoccupied d states associated with Pt/C E-TEK and Pt_2Sn_1/C at 1,100 mV (and Pt foil), respectively: 0.3489, 0.3167, (and 0.3 for Pt foil). The analysis done with the method of Shukla et al. [9] gave some information about the d-band vacancies through the integrated intensity of the Lorentzian, i.e., 0.00794 keV for Pt/C E-TEK at 1,100 mV, 0.00698 keV for Pt_2Sn_1/C at 1,100 mV and 0.00397 keV for Pt foil. Results from both techniques indicate that the presence of Sn in the Pt_2Sn_1/C catalyst causes a partial filling of the d band in relation to Pt/C E-TEK, as $h_{Tr} < h_T(Pt_2Sn_1/C) < h_T(Pt/C\ E-TEK)$ and, analogously, the integrated intensity of the Lorentzian for Pt foil is smaller than that for Pt_2Sn_1/C, which in turn, is smaller than that for Pt/C E-TEK. Sn is considered to enhance the activity of Pt in the anode by the formation of oxide/hydroxide species. However, the results of this work show that there is also a significant electronic effect when Sn is alloyed to Pt.

The adsorption phenomenon of reagents and intermediates in electrocatalytic processes basically consists of the transference of charge either to or from the catalyst metal (the substrate) with the participation of an atom, molecule, or ion (the adsorbate). Thus, it becomes clear that the electrical properties of the substrate are of crucial concern regarding the whole adsorption process, more specifically in relation to the adsorption enthalpy. To study and design new electrocatalytic materials with a desired property, e.g.,

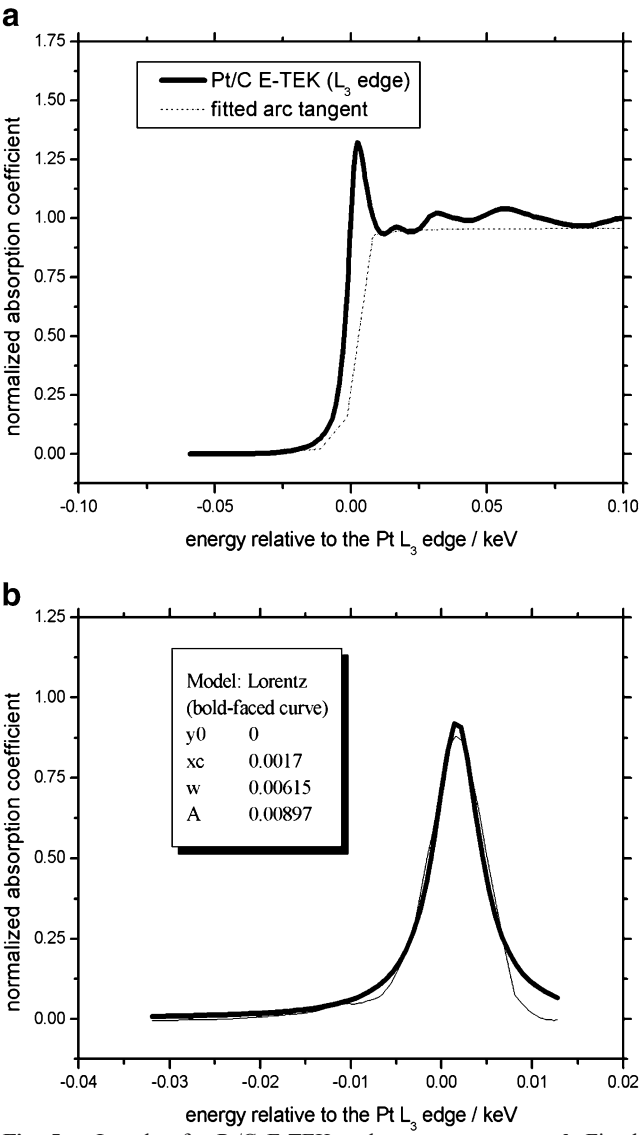

Fig. 5 **a** L_3 edge for Pt/C E-TEK and arc tangent curve. **b** Fitted Lorentzian for Pt/C E-TEK at 1,100 mV

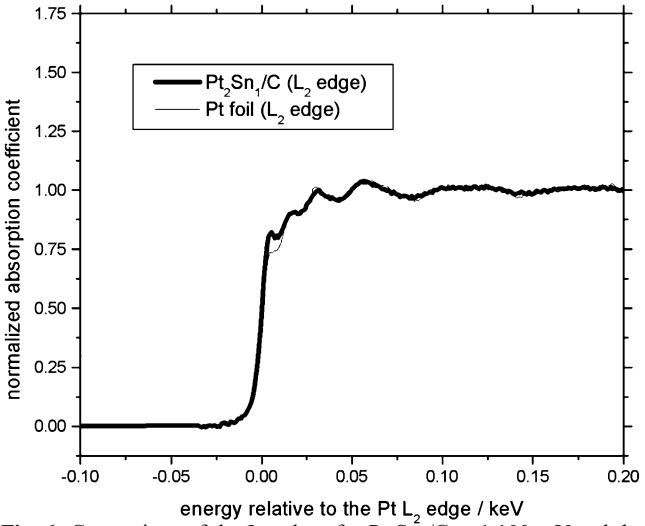

Fig. 6 Comparison of the L_2 edges for Pt_2Sn_1/C at 1,100 mV and the reference material (Pt foil)

low interaction with poisonous species like CO, it is important to use adequate techniques that supply information on the vacancy of specific orbitals (in terms of electronic density) of the catalyst that will interact with the adsorbate and, thus, gaining knowledge on the interactions between the adsorbate and the substrate. As described in this work, the XANES region can provide qualitative and quantitative information related to the electronic density of states of the studied materials. Focusing on PEMFC electrocatalytic processes, a low filling of Pt orbitals could reduce the electronic density shared by the metal surface and the adsorbed poisonous species, such as CO, in the anode of a H_2/O_2 low-temperature fuel cell, thus, weakening the adsorption strength. This phenomenon is generally called "electronic effect," and several platinum-based alloys have been

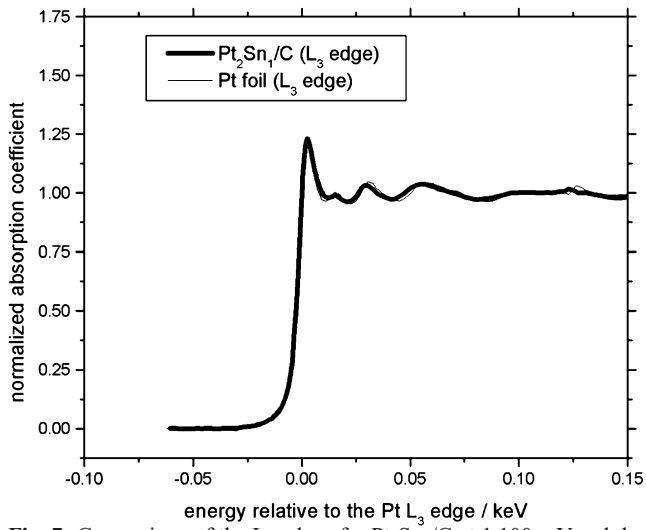

Fig. 7 Comparison of the L_3 edges for Pt_2Sn_1/C at 1,100 mV and the reference material (Pt foil)

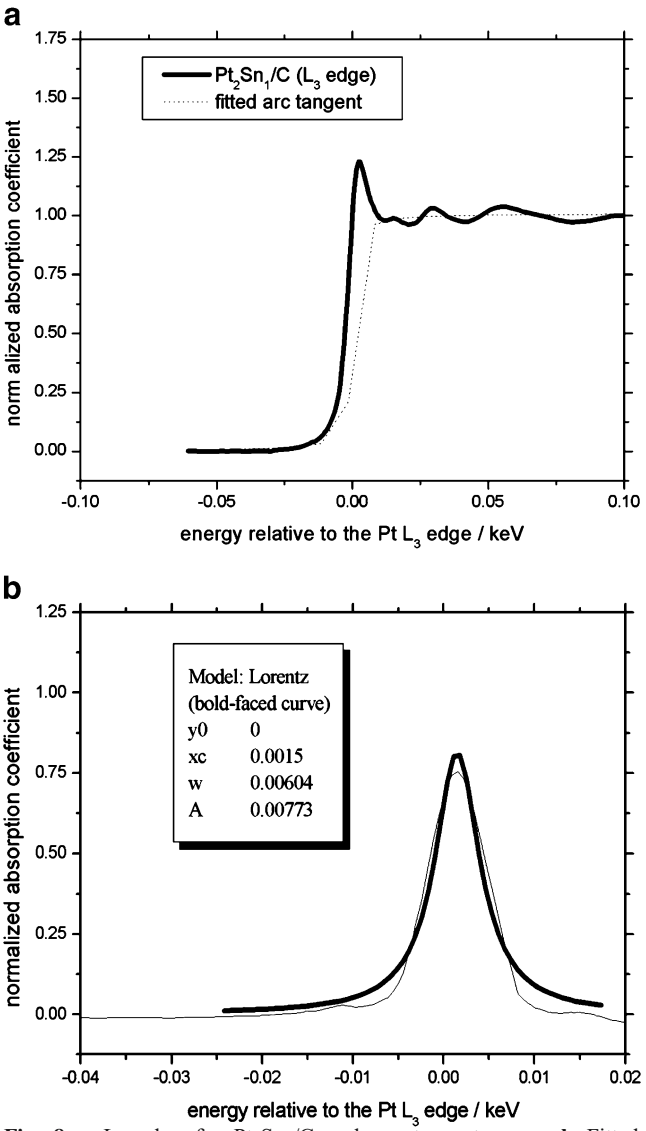

Fig. 8 **a** L_3 edge for Pt_2Sn_1/C and arc tangent curve. **b** Fitted Lorentzian for Pt_2Sn_1/C at 1,100 mV

proposed to decrease the adsorption strength of CO and, thus, decrease its poisoning effect [27–29].

The results presented in this work show that Pt in the Pt_2Sn_1/C bimetallic material presents, at the same electrode potential, more filled d orbitals than Pt/C E-TEK, as indicated both by a lower number of unoccupied states (Mansour's method) and by the smaller values of the integrated intensity of the Lorentzian (Shukla's approach). This behavior is consistent with the work of Mukerjee et al. [6], where the authors concluded that the decrease in the Pt 5d-band vacancies can be attributed to a donation of electrons from the Sn 5p and s bands to the Pt 5d band, which is a powerful acceptor. The results found experimentally are also in agreement with theoretical molecular orbital calculations [30] that show that the donation of electrons by Sn to Pt is quite possible. Actually, Pt–Sn

bimetallic materials have been used also for the electrochemical oxidation of methanol and ethanol in direct alcohol fuel cells (DAFC). In both cases, the electrochemical performance of the fuel cell using Pt–Sn/C is better than with Pt/C.

Focusing on the practical techniques for the quantitative analysis of white lines, it is possible to observe that the main drawback of the method of Shukla et al. [9] seems to be the fact that it does not supply the number of unoccupied d states, but only some integral values. Thus, the results are qualitative. When using the methodology of Mansour et al. [5], the results are quantitative, but there is some uncertainty in scaling and positioning the energy of the edges. In some cases, e.g., when there are only experimental data associated with the L_3 edge, one can take advantage of Shukla's approach [9], as it does not require information about the L_2 edge (and, in this sense, it is simpler to use). However, care must be taken regarding the fitting of the parameters because the arc tangent function constants are not arbitrary. As stated above, for the non-XAS specialist, the interpretation of XANES spectra to derive the desired information may be an arid process that can be facilitated following the procedures described in detail in this work.

Finally, it is important to point out that the treatments presented in this paper have some limitations, and further considerations must be made in particular situations. In the case of nanometer-scale metallic clusters, it is important to consider structural parameters such as the size and morphology of the cluster. In this cases, the methodology presented in this paper can be applied to the white line corresponding to each type of metallic (e.g., platinum) atom of the cluster (central and surface atoms) [31, 32].

Conclusions

The analysis of XANES spectra using the method proposed by Mansour et al. [5] gave the number of unoccupied d states associated with Pt/C E-TEK and Pt_2Sn_1/C at 1,100 mV and with a Pt foil used as reference. The analysis by the method proposed by Shukla et al. [9] gave qualitative information about the d-band vacancies through the integrated intensity of fitted Lorentzians. Results from both techniques indicate that the presence of Sn causes a partial filling of the d-band vacancies in comparison to Pt/C E-TEK. Although the approach proposed by Shukla et al. [9] does not supply the number of unoccupied d states, but only some integral values, and the method of Mansour et al. [5] presents some uncertainties in the scaling and positioning of the energy of the edges, both techniques are useful to obtain information on the vacancy of d states of platinum in the metal and its alloys, which is very important fundamental information to analyze and compare electrocatalytic activities.

Acknowledgment The authors thank Fundação de Amparo à Pesquisa do Estado de São Paulo, Conselho Nacional de Desenvolvimento Científico e Tecnológico, and Coordenação de Aperfeiçoamento de Pessoal de Nível Superior for financial support and the Brazilian Synchrotron Light Laboratory (LNLS) for assisting with the XAS experiments.

References

1. Koningsberger DC, Prins R (1988) X-ray absorption: principles, applications, techniques of EXAFS, SEXAFS and XANES. Wiley–Interscience, New York, NY
2. Brown M, Peierls RE, Stern EA (1977) Phys Rev B 15:738
3. Mattheiss LF, Dietz RE (1980) Phys Rev B 22:1663
4. Antolini E, Salgado JRC, Giz MJ, Gonzalez ER (2005) Int J Hydrogen Energy 30:1213
5. Mansour AN, Cook JW, Sayers DE (1984) J Phys Chem 88:2330
6. Mukerjee S, McBreen J (1999) J Electrochem Soc 146:600
7. Russell AE, Maniguet S, Mathew RJ, Yao J, Roberts MA, Thompsett D (2001) J Power Sources 96:226
8. Ramallo-López JM, Santori GF, Giovanetti L, Casella ML, Ferretti OA, Requejo FG (2003) J Phys Chem B 107:11441
9. Shukla AK, Raman RK, Choudhury NA, Priolkar KR, Sarode PR, Emura S, Kumashiro R (2004) J Electroanal Chem 563:181
10. Weinberger P, Rosicky F (1978) Theor Chim Acta 48:349
11. Slater JC, Koster GF (1954) Phys Rev 94:1498
12. Horsley JA (1982) J Chem Phys 76:1451
13. Cook JW, Sayers DE (1981) J Appl Physi 52:5024
14. Newville M, Livins P, Yacoby Y, Rehr JJ, Stern EA (1993) Phys Rev B 47:14126
15. Wong J, Lytle FW, Messner RP, Maylor DH (1984) Phys Rev B 30:5596
16. Richtmyer FK, Barnes SW, Ramberg E (1934) Phys Rev 46:843
17. Pinheiro ALN, Oliveira Neto A, de Souza EC, Perez J, Paganin VA, Ticianelli EA, Gonzalez ER (2003) J New Mater Electrochem Syst 6:1
18. Warren BE (1969) X-ray diffraction. Addison–Wesley, Reading, MA
19. Mascarenhas YP, Pinheiro JMV (1985) Programa para Cálculo de Parâmetro de Rede pelo Método de Mínimos Quadrados, SBPC
20. Colmati F, Antolini E, Gonzalez ER (2007) Appl Catal B 73:106
21. McBreen J, O'Grady WE, Pandya KI, Hoffman RW, Sayers DE (1987) Langmuir 3:428
22. Herron ME, Doyle SE, Pizzini S, Roberts KJ, Robinson J, Hards G, Walsh FC (1992) J Electroanal Chem 324:243
23. Hwang BJ, Tsai YW, Lee JF, Borthen P, Strehblow HH (2001) J Synchrotron Radiat 8:484
24. Ressler T (1997) J Physique IV 7:269
25. Marquardt DW (1963) J Soc Ind Appl Math 11:431
26. McMaster WH, Kerr Del Grande N, Hubell JH (1969) Compilation of X-ray cross-sections, National Technical Information Service, Springfield, VA
27. Liu P, Logadottir A, Norskov JK (2003) Electrochim Acta 48:3731
28. Koper MTM (2004) Surf Sci 548:1
29. Arenz M, Stamenkovic V, Blizanac BB, Mayrhofer KJ, Markovic NM, Ross PN (2005) J Catal 232:402
30. Anderson AB, Grantscharova E, Shiller P (1995) J Electrochem Soc 142:1880
31. Bazin D, Rehr JJ (2003) J Phys Chem B 107:12398
32. Bazin D, Sayers D, Rehr JJ, Mottet C (1997) J Phys Chem B 101:5332